Received: 17 May 2021 | Revised: 22 September 2021 | Accepted: 8 October 2021

DOI: 10.1002/app.51802

ARTICLE

Applied Polymer SCIENCE WILEY

Emulsion templated polymer monoliths containing cellulose nanocrystals: Synthesis and adsorption properties

Ali Eslek[1] | Burcu Kekevi[2] | Hatice Hande Mert[3] | Emine Hilal Mert[4]

[1]Department of Polymer Materials Engineering, Institute of Graduate Studies, Yalova University, Yalova, Turkey

[2]Material and Material Processing Department, Yalova Community College, Yalova University, Yalova, Turkey

[3]Department of Chemical Engineering, Faculty of Engineering, Yalova University, Yalova, Turkey

[4]Department of Polymer Materials Engineering, Faculty of Engineering, Yalova University, Yalova, Turkey

Correspondence
Emine Hilal Mert, Department of Polymer Materials Engineering, Faculty of Engineering, Yalova University, 77200 Yalova, Turkey.
Email: hmert@yalova.edu.tr

Abstract

Cellulose nanocrystals (CNCs) loaded hierarchical macroporous polymer monoliths were synthesized through high internal phase emulsion (HIPE) templating. For this purpose, unmodified CNCs were used as nanofiller in various amounts during HIPE preparation. The effect of CNCs loading on the hierarchical pore structure and mechanical properties was investigated. It was demonstrated that mechanical strength was significantly improved by CNCs loading. In order to reveal an application field, adsorptive property of resulting monoliths was investigated against Nile blue dye. The results showed that the maximum adsorption capacity of cationic Nile blue was 54% for the neat monolith, while it was 70% for the monolith prepared by 9 wt% CNCs loading. Meanwhile, the kinetic evaluation of the experimental adsorption data revealed that the adsorption follows pseudo-second-order kinetic model and it is consistent with Freundlich isotherm.

1 | INTRODUCTION

The adsorption capacity and the efficiency of an adsorbent vary depending on the chemical structure and porosity of the adsorbent. In this respect, while chemical structure is important to provide high content of functional groups for chemisorption, porosity and pore structure are important to increase the contact surface between the adsorbent and the pollutant. In addition, high porosity allows greater amounts of contaminants to penetrate the adsorbent.[1] For an efficient adsorption of toxic contaminants, polymer-based adsorbents are mostly preferred due to their eco-friendly nature, renewability, and reported superior performance.[2,3] In this respect, an effective strategy to synthesize well-defined macroporous polymers, which is known as high internal phase emulsion (HIPE) templating, is attracting valuable attention of the scientists.[4,5]

An HIPE is a concentrated emulsion containing an internal phase over 74.05 vol% of the total emulsion volume. Polymerization of HIPEs is usually achieved by the free radical polymerization of the monomer containing external phase. Thereby, resulting polymers are termed as "polyHIPE"s.[4–6] Depending on the highly porous and permeable structure, polyHIPEs offer many advantages in adsorption, ion-exchange, and chromatography applications.[4,7,8] However, low foam density and mechanical strength resulting from the porous structure is a disadvantage of these materials.[6] Another disadvantage of polyHIPEs arises from the limitations of thermodynamic emulsion stability. Monomers, which allow further chemical functionalization reactions with their suitable sites, have polar characters. For this reason, used monomers might compromise emulsion stability.[9]

In the last two decade, researchers have been demonstrated synthesis of functional polyHIPEs by using several polar monomers, such as glycidyl methacrylate (GMA)[9,10] and 2-hydroxyethyl methacrylate (HEMA).[11] The main strategy for the preparation of functional polyHIPEs is focused on further functionalization of the resulting polyHIPE with the use of modifying chemical agents. On the other hand, incorporation of nanoparticles

   J Appl Polym Sci. 2022;139:e51802. https://doi.org/10.1002/app.51802

has also been demonstrated as a successful approach to prepare functional polyHIPEs. Depending on their types and properties, incorporation of nanoparticles might bring additional advantages. For instance, nanoclays,[12] nanosilica particles,[13] cellulose nanocrystals (CNCs),[14] or nanoparticles such as Fe_2O_3,[15] TiO_2,[16–18] and ZnO[19] have been successfully used in the HIPE templating.

CNCs can be used as reinforcing agents for the preparation of polymer composites and nanocomposites. In addition to improving mechanical properties, they can also enhance thermal and morphological properties and add functionality to resulting materials.[20–22] On the other hand, because CNCs are highly hydrophilic, the main problem is the low compatibility between polymer chains and cellulose units.[23] For this purpose, surface functionalization is used as an effective approach to overcome this drawback. With this way, interaction between the phases can be increased.[14,22] On the other hand, previous studies had shown that the adsorption capacity of cellulose was increased dramatically after chemical treatment.[24] In this respect, the adsorption efficiency of CNCs against Cu(II) and Victoria blue dye was demonstrated by the researchers.[25] By this study, it was shown that by loading poly(ether sulfone) (PES) membranes with only 1 wt% of CNCs increased the adsorption efficiency of the PES membrane up to 99%.

Herein, macroporous polyHIPE monoliths containing unmodified CNCs were synthesized for removing cationic Nile blue dye from aqueous solutions. For this purpose, polyHIPE synthesis was achieved by the copolymerization of styrene (S), divinylbenzene (DVB), and 1,4-butanediol diacrylate (BuDAc) within the continuous phase of water-in-oil (w/o) type HIPEs. By using BuDAc in the monomer composition, compatibility of unmodified CNCs with the monomer containing continuous phase was partially improved. Efforts were made to improve the mechanical and thermal properties of the polyHIPE monoliths by CNCs loading, and without compromising hierarchical pore morphology. It was shown that using unmodified CNCs has a significant contribution on the final polyHIPE properties and the adsorption capacity. As a result, it has been shown that CNCs loaded polyHIPE monoliths can be prepared without the need for the surface modification step that increases the cost and reduces the overall benefit.

2 | EXPERIMENTAL SECTION

2.1 | Materials

Styrene (S) (Merck), divinylbenzene (DVB) (80%, Aldrich), 1,4-butanediol diacrylate (BuDAc) (technical grade, contains ~75 ppm hydroquinone as inhibitor, Sigma-Aldrich), crystalline nanocellulose (CNC) (dry powder, Dia:10–20 nm, L:300–900 nm, Nanografi) sorbitan monooleate (Span® 80) (non-ionic surfactant, Aldrich Chemistry), Pluronic® L121 (poly (ethyleneglycol)-block-poly(propyleneglycol)-block-poly (ethyleneglycol), Mn ~ 4400, non-ionic surfactant, Aldrich), potassium persulfate (KPS; ≥99.0%, ACS reagent), calcium chloride hexahydrate ($CaCl_2.6H_2O$; 98%, Sigma-Aldrich), Nile blue A (dye content ≥75%, Merck), and ethanol (technical grade) were used as received. In all experiments, ultrapure double distilled deionized water was used.

2.2 | Synthesis of poly(styrene-*co*-divinylbenzene-*co*-butanediol diacrylate) (PSBuDAc) monolith

Macroporous PSBuDAc monolith was prepared by using HIPE templating approach. For this purpose, HIPEs were prepared by dispersing 80 vol% of internal phase in 20 vol % of continuous phase, which was composed of monomers and emulsifiers. Where, the monomer mixture was composed of styrene, DVB, and BuDAc at a ratio of 80/15/5, respectively. On the other hand, the amount of Span® 80 was corresponding to 95 vol% of the continuous phase, while Pluronic® L121 was used 5 vol% with regard to the continuous phase. Briefly, a two-necked round-bottom flask equipped with an overhead stirrer and peristaltic pump inlet was charged with styrene (7.248 g), DVB (1.371 g), BuDAc (0.525 g), Span® 80 (2.8101 g), and Pluronic® L121 (0.1509 g). Then 40 mL of aqueous phase consisting of potassium persulfate (0.2237 g) and $CaCl_2.6H_2O$ (0.40 g) was added by peristaltic pump with a pumping rate of 50 rpm, under constant stirring (300 rpm). The resulting cream-like viscous emulsion was stirred for an additional 30 min, in order to provide homogeneous distribution of the droplet phase. Then, it was removed into a cylindrical glass container and kept in an air circulated oven for 24 h (@60°C) for the completion of crosslinking. The cover of the glass container was kept closed during this procedure. Crosslinked white colored monolith was Soxhlet-extracted in ethanol for 24 h and dried in a vacuum oven (@40°C) until constant weighing was available.

2.3 | Synthesis of CNC loaded PSBuDAc monoliths

Synthesis of CNCs loaded PSBuDAc monoliths was achieved by using a similar procedure described in Section 2.2. The only difference was the addition of 1, 3,

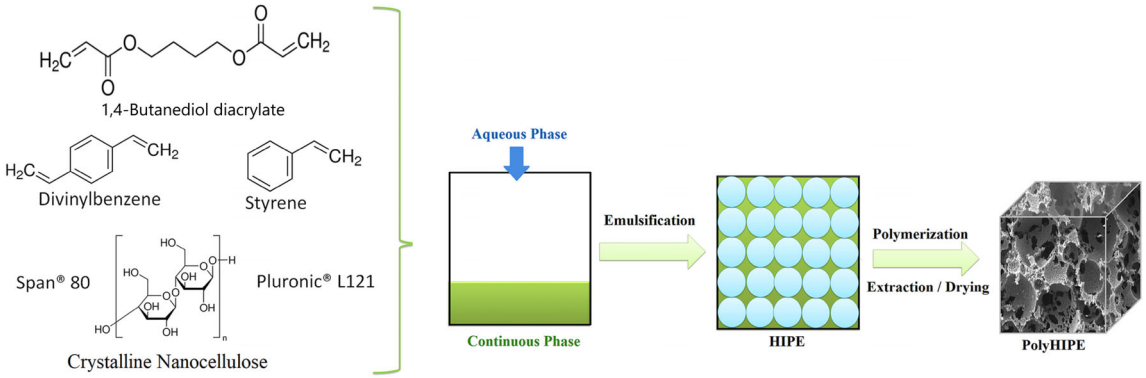

FIGURE 1 Schematic representation of monolith synthesis [Color figure can be viewed at wileyonlinelibrary.com]

7, or 9 wt% of CNCs into the monomer containing continuous phase, before the addition of the aqueous phase. Once the CNCs were added, the continuous phase was stirred for 15 min before the addition of the aqueous phase. Resulting monoliths were designated as PSBuDAc-Cx. In this naming, C is denoting CNCs and x is the weight percentage of CNCs. Synthesis of monoliths is schematized in Figure 1.

2.4 | Removal of Nile blue from aqueous solution

Adsorption of Nile blue (cationic dye) from aqueous solution was studied by using the synthesized macroporous monoliths as adsorbent via carrying out ultraviolet/visible measurements. Batch adsorption experiments were conducted in a set of 250 mL Erlenmeyer flasks containing monoliths and 100 mL of Nile blue solution at pH of 5.5 with an initial concentration of 1.0×10^{-5} M. The flasks were agitated on a shaker at 200 rpm and 30°C until equilibrium was reached. In order to calculate the removal of Nile blue, concentration of the dye was measured periodically at the wavelengths of $\lambda_{max} = 635$ nm by using a T80 + UV–VIS spectrophotometer (PG Instruments Ltd). The amount of adsorbed Nile blue, sorption efficiency (R %), and the percentage of removal were calculated using the following equations:

$$q_t = \frac{(C_0 - C_t).V}{m} \quad (1)$$

$$R(\%) = \frac{(C_0 - C_t)}{C_0} \times 100 \quad (2)$$

In these equations, C_o and C_t (mg/L) are the initial and the final concentrations of Nile blue, respectively. V is the volume of the solution (L), m is the weight of adsorbent (g), and q_t (mg/g) is the amount of adsorbed Nile blue at the end of the time.

2.5 | Characterization

Structural characterization of the polyHIPEs was performed by using Perkin Elmer Spectrum 100 FT-IR and water contact angle (WAC) test was performed with an Attension Theta Goniometer. Porous structure of the polyHIPE monoliths was investigated by scanning electron microscopy (SEM). For this purpose, morphology of the PSBuDAc monolith was determined by using FEI Inc., Inspect S50 model SEM, and EDAX, while morphologies of the PSBuDAc-Cx monoliths were determined by using ESEM-FEG and EDAX Philips XL-30 microscope. For SEM imaging, samples of 1 mm × 1 mm in size were mounted on a copper stub and coated with gold. Average cavity size and interconnected pore size of the obtained monoliths were also calculated by using SEM images with identical magnifications. For this purpose, diameters of at least 50 cavities were measured from the SEM image of each sample and then corrected by multiplying with a correction factor ($2/3^{1/2}$) to eliminate the influence of irregular cutting of samples.[6] Afterward, average cavity diameters were calculated with statistical errors. The same approach was also used for the calculation of interconnected pore size.

Mechanical properties of the polyHIPE monoliths were investigated in terms of compressive properties. With this aim, uniaxial compression tests were performed to cylindrical testing samples at a rate of 1.3 mm/min, under 10 kN compressive load. Compression tests were performed according to the ASTM D1621–2004 standard, by using Zwick/Roell Z020 Universal Testing Machine (Zwick GmbH &Co.KG). All measurements were repeated with three different specimens with specific dimensions of 15 mm in diameter and 10 mm in height.

Accordingly, stress versus strain plots were drawn by using the original data obtained from the testXpert II Testing software (Zwick GmbH &Co.KG). Compressive modulus of each sample was calculated from the initial slope of the stress–strain plots, while the compressive strength was defined as the maximum strength at the end of the initial linear elastic region. Specific compressive moduli and specific compressive strengths were obtained by normalizing the stress values by the individual foam densities.

Foam densities of the polyHIPE monoliths were calculated according to the Archimedes' principle by using an analytical balance equipped with a density determination kit (Sartorius YDK01).

3 | RESULTS AND DISCUSSION

3.1 | Synthesis and characterization of CNCs loaded polyHIPE monoliths

To investigate the influence of loading unmodified CNCs on the morphological, physiochemical, and mechanical properties of polyHIPE monoliths, the neat PSBuDAc and CNCs loaded PSBuDAc-Cx monoliths were synthesized with a nominal porosity of 80%. In order to improve the compatibility of the unmodified CNCs, continuous phase of the HIPEs was prepared with a monomer mixture composed of styrene, DVB, and BuDAc with a ratio of 80:15:5, respectively. Accordingly, polymerization of the continuous phase of HIPEs resulted in solid monolithic materials in all cases. After purification and drying steps, chemical structure, wettability, pore morphology, and mechanical properties of the obtained polyHIPE monoliths were investigated, depending on the amount of CNCs loading.

The chemical structure of the neat PSBuDAc and CNCs loaded PSBuDAc-Cx monoliths was investigated by FTIR analysis and the FTIR spectra of CNCs, PSBuDAc, and PSBuDAc-Cx monoliths are presented comparatively in Figure 2. In Figure 2, the characteristic peaks of CNCs, which were detected at 2356, 1585, 1411, 1302, and 1031 cm^{-1}, are to verify the incorporation of CNCs into the polyHIPE network.[26] The peak appeared at 2356 cm^{-1} arises due to C–O–C stretching of cellulose and the intensity of this peak increased depending on the amount of CNCs loaded in the PSBuDAc-Cx monoliths.[27] Hence the highest intensity was observed in the spectra of PSBuDAc-C9 monolith, as expected. C-H bending and stretching of CNCs clearly observed as a three-medium-intense sharp peak at 1585, 1411, and 1302 cm^{-1}, respectively. However, by loading CNCs, the intensity of that peaks lowered due to high –C–H vibrations not only coming from CNCs but also arising by the presence of BuDAc. Additionally, –C–O bending of CNCs detected at 1031 cm^{-1} lowered but the vibrations below that region (400–900 cm^{-1}) became clear and sharpened due to the intense vibrations of –C–H groups coming from the benzene ring of styrene and DVB.[28] Similarly, three medium-intense sharp peaks detected at 3024, 2912, and 2837 cm^{-1} also correspond to the –C–H stretching of the benzene ring in styrene and DVB.

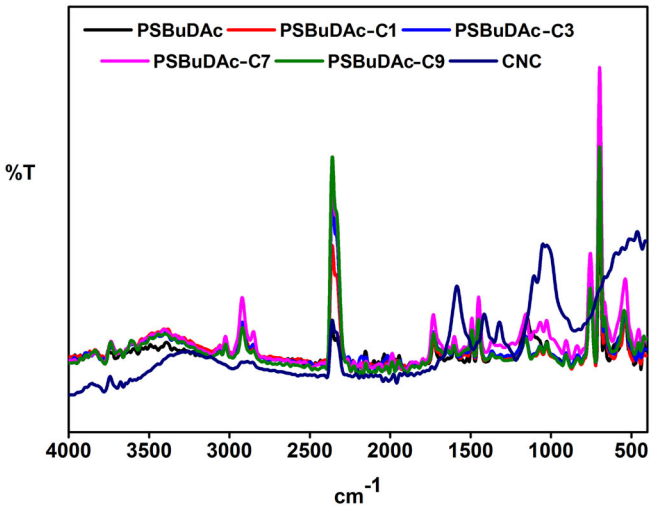

FIGURE 2 FTIR spectra of CNCs, PSBuDAc, and PSBuDAc-Cx monoliths [Color figure can be viewed at wileyonlinelibrary.com]

In order to clarify the attribution of hydrophilicity of CNCs on the surface properties of PSBuDAc-Cx monoliths, WAC measurements were performed. To make a reliable comparison, contact angle measurement was also carried out for the neat PSBuDAc monolith. The results of contact angle measurements are given in Table 1. It is known that, generally a contact angle at around or over 120° reflects the hydrophobicity of a polyHIPE.[29,30] In this respect, the contact angle of a 2.59 μL sessile water on PSBuDAc monolith, which was found to be 150.28 ± 1.03°, is verifying the hydrophobicity of the synthesized material. In addition, the contact angle value did not change depending on the interaction of the surface water droplets. For the PSBuDAC-Cx monoliths, it was determined that increasing the ratio of CNCs decreased the contact angle value of the water droplets. It was observed that, even though the presence of CNCs could not be able to hydrophilize all the surface, the contact angle decreased evidently by the alignment of CNCs in polyHIPE network.[31,32] However, the hydrophobic nature of the PSBuDAc-Cx monoliths was determined to be protected.

The macroporous morphologies of the monoliths were observed with SEM, and images of PSBuDAc and

TABLE 1 Morphological properties of the monoliths

Monolith	CNC (wt%)	Water contact angle (°)	Average cavity size (μm)	Average pore size (μm)
PSBuDAc	-	150.28 ± 1.03	42.75 ± 1.11	10.10 ± 0.42
PSBuDAc-C1	1	149.61 ± 1.06	27.38 ± 0.86	8.06 ± 0.22
PSBuDAc-C3	3	143.07 ± 1.21	28.34 ± 1.15	8.12 ± 0.31
PSBuDAc-C7	7	140.15 ± 1.15	19.75 ± 0.88	6.21 ± 0.31
PSBuDAc-C9	9	136.42 ± 1.16	16.23 ± 0.59	6.00 ± 0.21

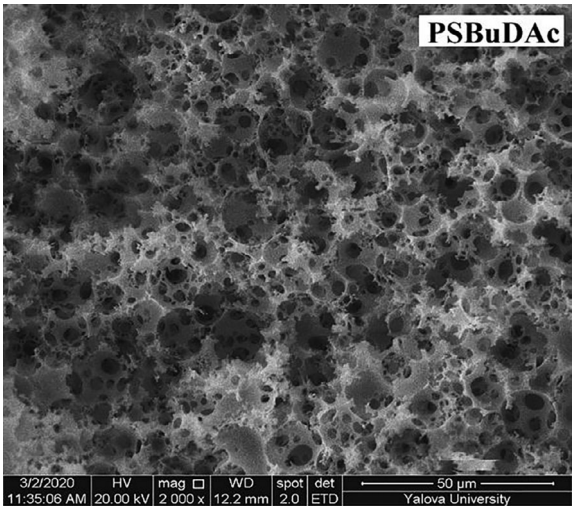

FIGURE 3 SEM image of the PSBuDAc monolith

PSBuDAc-Cx monoliths are presented in Figures 3 and 4, respectively. As can be seen in Figure 3, the SEM image of the PSBuDAc monolith clearly conforms to the hierarchical morphology of emulsion-template monoliths. The neat PSBuDAc monolith is highly open porous and the surface of this monolith is very smooth. According to Table 1, the average cavity size and pore size calculated from the SEM image of PSBuDAc are 42.75 and 10.10 μm, respectively. On the other hand, Figure 4 shows the pore morphologies of the PSBuDAc-Cx monoliths. As it can be seen from the images presented in Figure 4 that PSBuDAc-Cx monoliths containing various amounts of CNCs changing between 1 wt% and 9 wt% are exhibiting a hierarchical pore morphology. It can also be seen that due to CNCs contribution, the surfaces of these monoliths are rougher compared to the neat PSBuDAc monolith.

As can be noticed from the SEM images, the hierarchical pore morphology was not compromised even when the CNC loading amount reached 9% by weight. This result is important when emulsion stability is considered. It is well known that emulsions are thermodynamically unstable complex systems. Stability of an emulsion depends on the emulsion phases, surfactant type and amount, temperature, energy input, and other components such as nanoparticles. In case of HIPEs, emulsion destabilization processes such as coalescence and Ostwald ripening usually occurred at high temperatures during polymerization of the continuous phase and cause collapse of the pores.[33] On the other hand, using nanoparticles or polar monomers can accelerate coalescence and Ostwald ripening of the emulsion droplets. Nanoparticles generally used after increasing the compatibility with the emulsion phases by surface modification. Thereby, obtaining monoliths without compromising hierarchical pore structure by the addition of unmodified CNCs ranging between 1 wt% and 9 wt% might be considered as a remarkable result.

It is known that a hydrophilic property of CNCs is the main problem when they are loaded into hydrophobic polymer matrices. Similarly, the addition of CNCs into hydrophobic continuous phase of HIPEs might result in emulsion destabilization or disruption of pore morphology of polyHIPEs. In here, by using BuDAc in the continuous phase preparation, the compatibility between CNCs and the monomer phase was increased. When the morphological properties of PSBuDAc-Cx monoliths were compared with those of PSBuDAc, the addition of CNCs was found to significantly reduce the average cavity size and pore size (Table 1). Increasing the amount of CNCs loading from 1 wt% to 9 wt% resulted in ~40% of decrement in the average cavity size and ~ 26% of decrement in the average pore size. In addition, as compared to the PSBuDAc monolith, it was determined that the addition of 9 wt% CNCs to the polyHIPE matrix reduced the average cavity size by 62% and the average pore size by 40%. It can be concluded from these results that the increase in the amount of CNCs loading caused decrease in the average cavity size and pore size, which can be attributed to the increased emulsion stability. The stability of HIPEs has a significant role on the determination of final pore morphology. HIPEs should have maintained stability during polymerization.[33] In the case of lower emulsion stability, Ostwald ripening and coalescence are the two main mechanisms that play a significant role in destabilization process. The result of emulsion destabilization

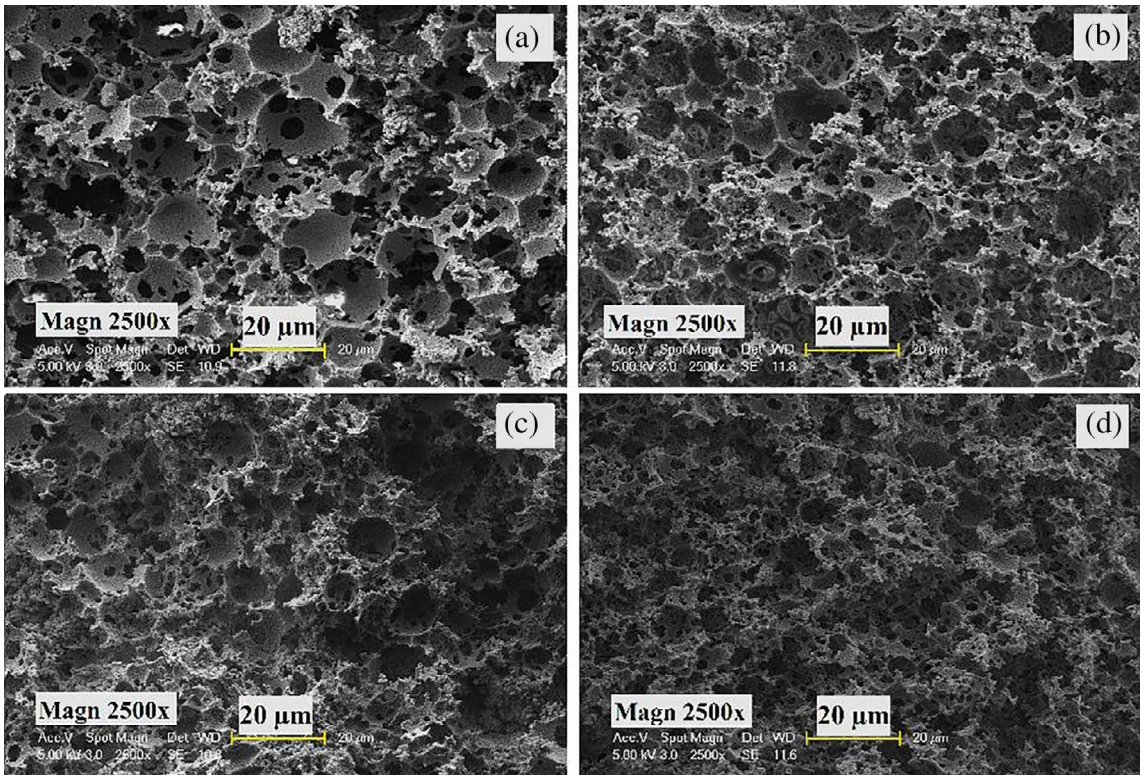

FIGURE 4 SEM images of PSBuDAc-Cx monoliths. (a) PSBuDAc-C1. (b) PSBuDAc-C3. (c) PSBuDAc-C7. (d) PSBuDAc-C9 [Color figure can be viewed at wileyonlinelibrary.com]

mechanisms, on the other hand, is the increase in the average droplet size of emulsions.[33] After polymerization, increasing droplet size results in the formation of larger cavities. In this study, addition of BuDAc into the monomer mixture did not compromise emulsion stability, while improving the compatibility between the monomer phase and the CNCs. From the comparison of the SEM images of PSBuDAc-Cx monoliths presented in Figure 4 in relation with the amount of CNCs loading, it can be concluded that the smaller cavities are formed with the increasing amount of CNCs. Furthermore, it can be also concluded that increasing CNCs loading leads to an increase in the interconnectivity of cavities. This result can be explained by thinning of continuous polymer film around the droplets, which is a result of increasing share of the droplet phase.[9,32,34]

Since porous structure brings significant advantages such as high permeability and convective mass transfer, it is essential for many applications such as adsorption and separation processes, chromatography, and tissue engineering.[35] However, low mechanical strength is the main drawback of increasing the porosity level of a material. In the case of polyHIPEs, while the hierarchical morphology resulting from the two-level pore size offers several advantages in applications, the actual industrial applications of these materials are rather limited due to their low mechanical properties. In this respect, incorporation of neat CNCs into polyHIPE matrix is demonstrated as a convenient approach for the improvement of mechanical properties. Since the resulting monoliths are polymeric foams, variation of the mechanical properties by CNCs loading was investigated in terms of compression modulus. The compression modulus of the samples was determined by using the original data obtained from the software. Similarly, stress versus strain curves were also plotted by using the original data. Accordingly, the stress versus strain plots of the PSBuDAc and PSBuDAc-Cx monoliths are presented in Figure 5, while the compression moduli of each monolith are given in Table 2.

It can be clearly seen from Figure 5 and Table 2 that incorporating CNCs have had a significant contribution on the improvement of mechanical strength. Variation of the compression modulus of monoliths is in accordance with the stress–strain plots. Compression modulus of the neat PSBuDAc monolith was found to be 5.02 MPa, while the compression strength was 0.20 MPa. However, incorporation of CNCs at higher amounts than 1 wt% was resulted in a steady increase in both the compression modulus and strength. In this respect, compression modulus and strength of PSBuDAc-C9 were increased to 47.7 and 4.01 MPa, respectively. It is known from the previous literature that CNCs as fillers have numerous features

that are advantageous for improving the material properties including low density, high elastic modulus, and mechanical strength, and abundant hydroxyl groups.[36] CNCs supported polymer matrices demonstrate improved mechanical strength due to the transfer of the applied load from polymer matrix to CNCs.[37] On the other hand, although CNCs loading is highly advantageous because of the benefits it provides in terms of improving mechanical properties, in most cases the need for surface modification to increase compatibility with the polymer phase is a cost-increasing requirement that reduces the overall benefit.[36] In this study, the degree of increment in the compressive properties of the obtained monoliths demonstrates that the strength of polyHIPE matrices can be supported against compressive load to a certain extent by using CNCs without any surface modifications. However, it might be useful to discuss the observed increase in mechanical strength with CNCs loading along with the change of morphological features. In this respect, comparison of Tables 1 and 2 reveals that the increasing trend of compressive properties can be also attributed to the decrease in average cavity size with the increase in CNCs loading. From this point of view, it can be said that the increase in the compressive properties of the prepared CNCs incorporated polyHIPE monoliths is also related with the emulsion stability.

In order to reveal the influence of CNCs loading on thermal stability, thermo gravimetrical analysis of the resulting monoliths was also conducted. The results are presented in Supplementary Material file. It was concluded from the comparison of the obtained thermograms (see Figure S1) that incorporating CNCs did not make a significant difference in the thermal stability of the polyHIPE monoliths.

Incorporation of CNCs also resulted in an increase in the foam density. While the density of the PSBuDAc monolith was 0.25 g cm^{-3}, the density of PSBuDAc-C3 monolith was increased to 0.30 g cm^{-3} by the incorporation of 3 wt% CNCs. The increase in the density of the monoliths was found to be continued with the increase in the CNCs loading amount. Accordingly, the densities of PSBuDAc-C7 and PSBuDAc-C9 monoliths were determined as 0.35 and 0.36 g cm^{-3}, respectively. In order to obtain the specific compression modulus and specific crush strengths, the stress values were normalized by the individual foam densities and presented in Table 2. As compared to the neat PSBuDAc, specific compressive modulus and strength were increased significantly with the increase in the CNCs loading amount. As compared to PSBuDAc-C3, the negligible decrease in the specific compression modulus of the PSBuDAc-C7 monolith can be ascribed to the increase in the foam density from 0.30 to 0.35 g cm^{-3}. In addition to all, the increase in the specific compression modulus and strength of the resulting monoliths can be attributed to the integration of the CNCs with the polymer network through intermolecular forces.

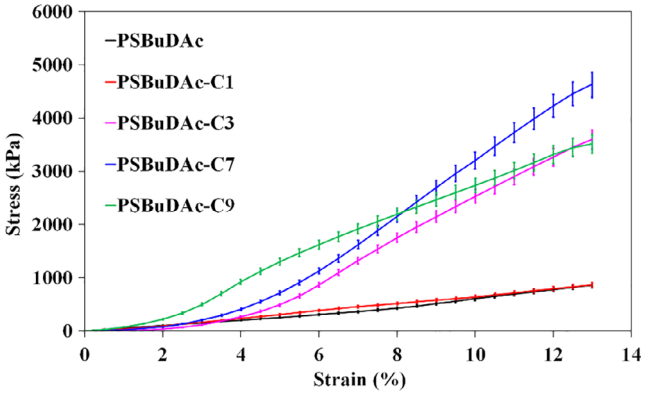

FIGURE 5 Stress versus strain plots of the PSBuDAc and PSBuDAc-Cx monoliths [Color figure can be viewed at wileyonlinelibrary.com]

3.2 | Adsorptive properties of CNCs loaded polyHIPE monoliths

Since one of the aims of this study is to designate an application field, the adsorptive properties of CNCs loaded polyHIPE monoliths was investigated by the removal of cationic Nile blue dye from aqueous solutions

TABLE 2 Foam density and compressive properties of the monoliths

Monolith	Foam density (g cm^{-3})	Compression modulus (MPa)	Compression strength (MPa)	Specific modulus (MPa g^{-1} cm^3)	Specific strength (MPa g^{-1} $cm^{3)}$
PSBuDAc	0.25	5.02	0.20	20.08	0.80
PSBuDAc-C1	0.25	6.74	0.51	26.96	2.04
PSBuDAc-C3	0.30	34.1	3.22	113.66	10.73
PSBuDAc-C7	0.35	37.6	3.77	107.43	10.77
PSBuDAc-C9	0.36	47.7	4.01	132.50	11.14

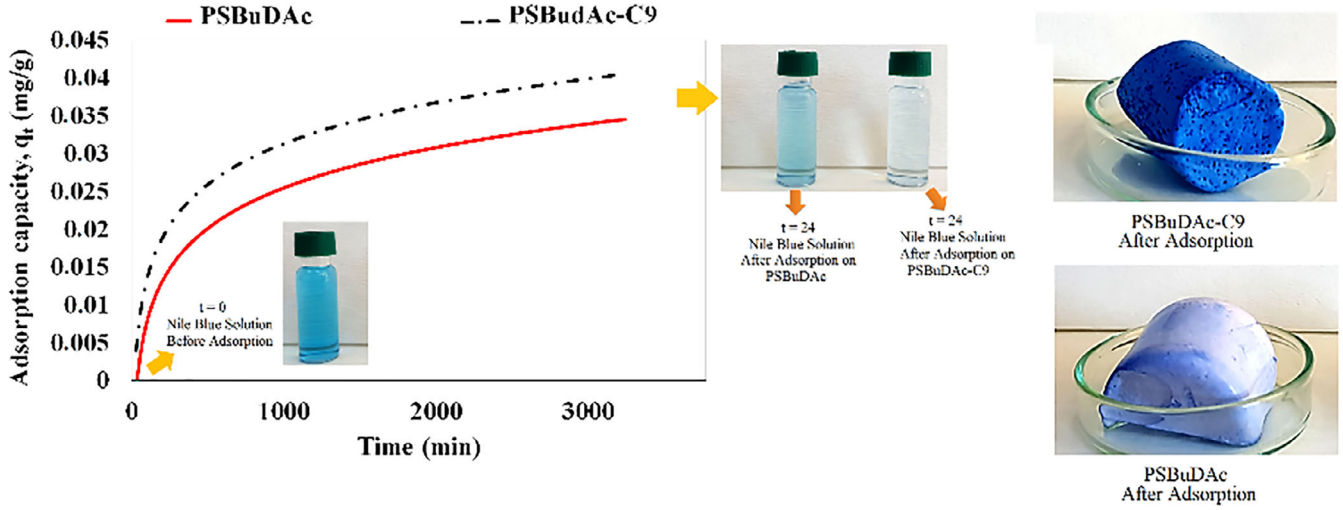

FIGURE 6 The adsorption performances of the PSBuDAc and PSBuDAc-C9 monoliths against cationic Nile blue dye in aqueous environment [Color figure can be viewed at wileyonlinelibrary.com]

using the obtained monoliths. For this purpose, morphological features and abundance of functional groups were considered while choosing the composite monolith in the adsorption experiments. Accordingly, PSBuDAc-C9 monolith containing 9% of CNCs by weight was used in the adsorption of Nile blue. It was expected here that the lower average cavity size and average pore size of PSBuDAc-C9 monolith might result in higher adsorption capacity. On the other hand, higher amounts of CNCs provide more –OH functionality and supports the formation of –H bridge bonds in the presence of a suitable solvent such as water. By formation of –H bridge bonds, monoliths can swell in the aqueous medium and this might ascend adsorption capacity by opening the distance between pores and creates additional surfaces for adsorption.[38] In order to demonstrate the influence of CNCs on the adsorptive properties, the neat PSBuDAc monolith was also examined for comparison.

The adsorption capacities of the monoliths were presented in Figure 6, comparatively. As can be seen from Figure 6, both monoliths display excellent adsorptive property with thanks to their macropores besides to the chemical composition of polyHIPE matrix. On the other hand, it was clearly seen that PSBuDAc-C9 monolith has higher adsorption capacity than the neat PSBuDAc monolith due to the presence of 9 wt% of CNCs. The adsorption capacity of PSBuDAc-C9 monolith was found to be 0.039 mg/g with 70% sorption efficiency, whereas PSBuDAc monolith performed an adsorption capacity of 0.033 mg/g with 54% sorption efficiency. This difference can be attributed to the presence of CNCs including several surface active hydroxyl (–OH) groups in the structure of PSBuDAc-C9 monolith.

3.3 | Kinetic evaluation of Nile blue adsorption onto the CNCs loaded polyHIPE monoliths

In order to investigate the kinetics of Nile blue removal two kinetic models, first-order (Equation 3)[39] and pseudo-second-order (Equation 4)[40] were tested by fitting the experimental data.

$$\frac{1}{q_t} = \left(\frac{k_1}{q_1}\right)\left(\frac{1}{t}\right) + \frac{1}{q_1} \tag{3}$$

$$\frac{t}{q_t} = \frac{1}{k_2 q_2^2} + \frac{1}{q_2} t \tag{4}$$

In the equations given above, q_1 and q_t are the amounts of dye adsorbed on the adsorbent monoliths at equilibrium and at various times t (mol g^{-1}) for the first-order

TABLE 3 Kinetic parameters for the adsorption of Nile blue onto PSBuDAc and PSBuDAc-C9 monoliths

	PSBuDAc	PSBuDAc-C9
First-order		
q_1 (mol g^{-1})	1.47×10^{-2}	7.49×10^{-2}
k_1 (min^{-1})	1.79×10^{2}	9.98×10^{2}
r^2_1	0.625	0.968
Pseudo second-order		
q_2 (mol g^{-1})	4.11×10^{-2}	4.32×10^{-2}
k_2 (mol L^{-1} min^{-1})	1.26×10^{7}	4.18×10^{6}
r^2_2	0.774	0.968

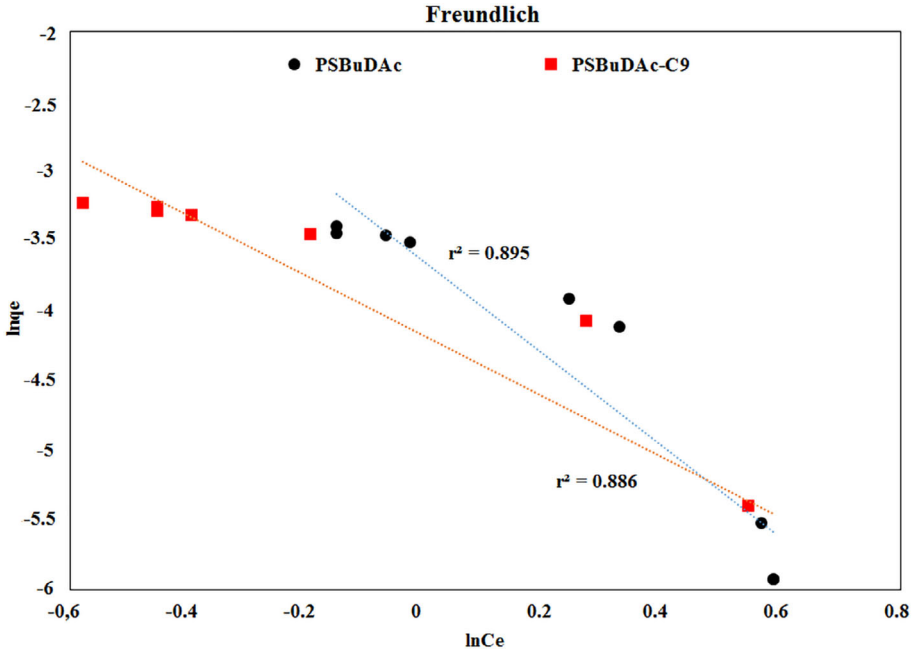

FIGURE 7 Freundlich isotherms for the adsorption of Nile blue onto the PSBuDAc and PSBuDAc-C9 monoliths [Color figure can be viewed at wileyonlinelibrary.com]

TABLE 4 Isotherm constants for the adsorption of Nile blue onto PSBuDAc and PSBuDAc-C9 monoliths

	PSBuDAc	PSBuDAc-C9
Langmuir		
q_{max} (mol g^{-1})	1.82×10^{-3}	2.68×10^{-3}
K_L (L mol^{-1})	1.13	1.65
r^2_L	0.695	0.616
Freundlich		
K_F (L g^{-1})	2.56×10^{-2}	1.52×10^{-2}
n	0.30	0.46
r^2_F	0.895	0.887

model adsorption, while q_2 (mol g^{-1}) is the maximum adsorption capacity for the pseudo-second-order adsorption. k_1 (min^{-1}) and k_2 (mol L^{-1} min^{-1}) are, respectively, the first-order and pseudo-second-order rate constants. By using the experimental data, the straight-line plots of $1/q_t$ versus $1/t$ (for the first-order reaction) and t/q_t versus t (for the pseudo-second-order reaction) for the adsorption of Nile blue onto PSBuDAc and PSBuDAc-C9 monoliths have been tested. Accordingly, kinetic parameters for the adsorption of Nile Blue were calculated from the plots and presented in Table 3. As can be seen the correlation coefficients of the plots for the first-order model (r^2_1) were found to be 0.625 and 0.968 for PSBuDAc and PSBuDAc-C9, respectively. On the other hand, the correlation coefficients of the plots for the pseudo-second-order model (r^2_2) were determined respectively as 0.774 and 0.968, for PSBuDAc and PSBuDAc-C9. According to these results, the kinetics of Nile blue adsorption onto the monoliths follows pseudo-second-order model, which is based on the assumption that chemisorption is the rate-limiting step during the adsorption process and the interaction between the sorbate molecule and the adsorption site controls the process.[41] On the other hand, the correlation coefficients for the first-order and pseudo-second-order models were found to be equal to each other for PSBuDAc-C9 and showed a great agreement with the experimental results.

To identify the adsorption isotherms, experimental data were fitted to Langmuir (Equation 5) and Freundlich (Equation 6) equations[40]:

$$\frac{1}{q_e} = \left(\frac{1}{q_{max} K_L}\right)\frac{1}{C_e} + \frac{1}{q_{max}} \quad (5)$$

$$lnq_e = lnK_F + \frac{1}{n} lnC_e \quad (6)$$

In these equations, q_e (mol g^{-1}), C_e (mol L^{-1}), and q_{max} (mol g^{-1}) are, respectively, the equilibrium Nile blue concentration on the adsorbent monoliths, the equilibrium Nile blue concentration in solution, and the monolayer capacity of the adsorbent monoliths, whereas K_L (L mol^{-1}) and K_F (L g^{-1}) are, respectively, the Langmuir and Freundlich constants. n (dimensionless) is the heterogeneity factor and its value changes by surface heterogeneity. The value of n indicates the nature of the adsorption process. When $n < 1$, the process is physical and if $n = 1$ and $n > 1$, it will be chemical and linear in nature.[42] By fitting the experimental data for Nile blue adsorption on PSBuDAc and PSBuDAc-C9 monoliths,

Langmuir (not shown) and Freundlich isotherms (Figure 7) were plotted, and kinetic parameters are given in Table 4. As can be seen from Table 4, the fit of the kinetic data suggests that the adsorption of Nile blue on PSBuDAc and PSBuDAc-C9 monoliths is closer for Freundlich model. This suggests that adsorption is in progress on heterogeneous surfaces with different affinities, and consistent with the previous findings reported for Nile blue adsorption in the literature.[43–45]

4 | CONCLUSION

In this study, unmodified CNCs were directly used in the synthesis of polyHIPE monoliths. By adding 5 vol% of flexible 1,4-butanediol diacrylate monomer into the hydrophobic continuous phase, stable HIPEs were obtained in the presence of CNCs. Preparation of the polyHIPE monoliths containing CNCs was achieved without compromising pore morphology. Thanks to the flexible diacrylate monomer and CNCs, mechanical properties of the monoliths were significantly improved. In other words, integration of the CNCs into the polymer network was supported by the significant increase of the specific compression modulus and strength of the polyHIPE monoliths. Adsorptive properties of polyHIPE monoliths were also investigated by removing Nile blue from aqueous solution. It has been shown that not only the monolith containing 9 wt% CNC (PSBuDAc-C9) but also the neat monolith (PSBuDAc) has an excellent adsorption capacity with thanks to the proper composition of polymer matrix and its obtained macroporous architecture. Moreover, the kinetics of Nile blue adsorption onto the PSBuDAc and PSBuDAc-C9 monoliths was also investigated. It was found that adsorption onto the monoliths follows pseudo-second-order model. Whereas, the results suggested that the adsorption process in progress on heterogeneous surfaces with different affinities and adsorption is closer for Freundlich model isotherm. We believe that resulting polyHIPE monoliths are good candidates as adsorbents for wastewater treatment.

ORCID

Ali Eslek https://orcid.org/0000-0003-1242-6087
Burcu Kekevi https://orcid.org/0000-0002-2364-1957
Hatice Hande Mert https://orcid.org/0000-0003-0743-1981
Emine Hilal Mert https://orcid.org/0000-0003-4267-7469

REFERENCES

[1] T. Luo, H. Liang, D. Chen, Y. Ma, W. Yang, *Appl. Surf. Sci.* **2020**, *505*, 144607.
[2] E. N. Zare, A. Motahari, M. Sillanpää, *Environ. Res.* **2018**, *162*, 173.
[3] F. S. Mustafa, M. Güran, M. Gazi, *J. Polym. Res.* **2020**, *27*, 247.
[4] T. Zhang, R. A. Sanguramath, S. Israel, M. S. Silverstein, *Macromolecules* **2019**, *52*, 5445.
[5] I. Pulko, P. Krajnc, Porous polymer monoliths by emulsion templating. in *Encyclopedia of Polymer Science and Technology*, John Wiley & Sons, Inc, Hoboken, NJ **2017**, p. 1.
[6] H. H. Mert, M. S. Mert, E. H. Mert, *Mater. Res. Express* **2019**, *6*, 115306.
[7] J. Luo, Z. Huang, L. Liu, H. Wang, G. Ruan, C. Zhao, F. Du, *J. Sep. Sci.* **2020**, *44*, 169.
[8] N. San, E. H. Mert, D. Kaya, F. Çira, *Fresenius Environ. Bull.* **2016**, *5*, 3635.
[9] S. Jerenec, M. Šimić, A. Savnik, A. Podgornik, M. Kolar, M. Turnšek, P. Krajnc, *React. Funct. Polym.* **2014**, *78*, 32.
[10] P. Krajnc, N. Leber, D. Štefanec, S. Kontrec, A. Podgornik, *J. Chromatogr. A.* **2005**, *1065*, 69.
[11] S. Kovačič, D. Štefanec, P. Krajnc, *Macromolecules* **2007**, *40*, 8056.
[12] E. Yüce, E. H. Mert, S. Şen, S. Saygı, N. San, *J. Appl. Polym. Sci.* **2017**, *134*, 45522.
[13] M. R. Moghbeli, A. Khajeh, M. Alikhani, *Chem. Eng. J.* **2017**, *309*, 552.
[14] H. H. Mert, M. R. Moghbeli, S. Sajad, E. H. Mert, *React. Funct. Polym.* **2020**, *151*, 104572.
[15] A. Vílchez, C. Rodríguez-Abreu, J. Esquena, A. Menner, A. Bismarck, *Langmuir* **2011**, *27*, 13342.
[16] E. Yüce, F. N. Parın, P. Krajnc, H. H. Mert, E. H. Mert, *React. Funct. Polym.* **2018**, *130*, 8.
[17] Q. Wang, H. Ma, J. Chen, Z. Du, J. Mi, *J. Environ. Chem. Eng.* **2017**, *5*, 2807.
[18] A. Koler, P. Krajnc, *Colloid Polym. Sci.* **2019**, *297*, 799.
[19] S. Kovačič, A. Anžlovar, B. Erjavec, G. Kapun, N. B. Matsko, M. Žigon, E. Žagar, A. Pintar, C. Slugovc, *ACS Appl. Mater. Interfaces* **2014**, *6*, 19075.
[20] H. C. Chen, W. T. Y. Tze, F. C. Chang, *Cellulose* **2020**, *27*, 5757.
[21] K. Y. Lee, J. J. Blaker, R. Murakami, J. Y. Y. Heng, A. Bismarck, *Langmuir* **2014**, *30*, 452.
[22] S. Pérez, K. Mazeau, 2 Conformations, structures, and morphologies of celluloses. in *Polysaccharides: structural diversity and functional versatility* (Ed: S. Dumitriu), Marcel Dekker, New York **2005**, p. 41.
[23] Q. Xu, J. Yi, X. Zhang, H. Zhang, *Eur. Polym. J.* **2008**, *44*, 2830.
[24] C. M. Clarkson, S. M. E. A. Azrak, E. S. Forti, G. T. Schueneman, R. J. Moon, J. P. Youngblood, *Adv. Mater.* **2020**, *33*, 2000718. https://doi.org/10.1002/adma.202000718
[25] F. Rafieian, M. Jonoobi, Q. Yu, *Cellulose* **2019**, *26*, 3359.
[26] M. Tsuboi, *J. Polym. Sci.* **1957**, *25*, 159.
[27] M. Sain, S. Panthapulakkal, *Ind. Crop. Prod.* **2006**, *2*, 1.
[28] A. Alemdar, M. Sain, *Bioresour. Technol.* **2008**, *99*(6), 1664.
[29] S. Livshin, M. S. Silverstein, *J. Polym. Sci: Part A: Polym. Chem.* **2009**, *47*, 4840.
[30] T. Zhang, Q. Guo, *Chem. Eng. J.* **2017**, *307*, 812.
[31] R. Prathapan, J. D. Berry, A. Fery, G. Garnier, R. F. Tabor, *ACS Appl. Mater. Interfaces* **2017**, *9*(17), 15202.
[32] P. Daraei, N. Ghaemi, H. S. Ghari, *Cellulose* **2017**, *24*, 915.
[33] R. Foudazi, *React. Funct. Polym.* **2021**, *164*, 104917.

[34] H. Bai, X. Wang, Y. Zhou, L. Zhang, *Prog. Nat. Sci. Mater. Int.* **2012**, *22*, 250.
[35] D. Wu, F. Xu, B. Sun, R. Fu, H. He, K. Matyjaszewski, *Chem. Rev.* **2012**, *112*(7), 3959.
[36] R. Laghaei, H. Fashandi, S. M. Hejazi, S. Shaghaghi, A. Shamaei-Kashani, *J. Compos. Mater.* **2021**, *0*(0), 1.
[37] E. DiLoreto, E. Haque, A. Berman, R. J. Moon, K. Kalaitzidou, *Cellulose* **2019**, *26*, 4391.
[38] K. Y. Lee, Y. Aitomäki, L. A. Berglund, K. Oksman, A. Bismarck, *Compos. Sci. Technol.* **2014**, *105*, 15.
[39] A. Özcan, E. M. Öncü, A. S. Özcan, *Colloids Surf. A Physicochem. Eng. Aspects* **2006**, *277*, 90.
[40] S. Abbasi, H. Noorizadeh, *Carbon Lett.* **2017**, *23*, 30.
[41] E. G. Contreras, B. E. Martinez, L. A. Sepúlveda, C. L. Palma, *Adsorpt. Sci. Technol.* **2007**, *25*, 637.
[42] S. F. Saberzadeh, H. Esmaeili, B. Ramavandi, *BioTechniques* **2016**, *6*, 251.
[43] T. B. İyim, I. Acar, S. Özgümüş, *J. Appl. Polym. Sci.* **2008**, *109*, 2774.
[44] M. Ghoochian, J. Iran, *Toxicology* **2016**, *10*(3), 7.
[45] L. E. Crandon, K. M. Boenisch, B. J. Harper, S. L. Harper, *PLoS One* **2020**, *15*(6), e0233844.

SUPPORTING INFORMATION

Additional supporting information may be found in the online version of the article at the publisher's website.

How to cite this article: A. Eslek, B. Kekevi, H. H. Mert, E. H. Mert, *J. Appl. Polym. Sci.* **2022**, *139*(11), e51802. https://doi.org/10.1002/app.51802